ACS APPLIED MATERIALS & INTERFACES

RESEARCH ARTICLE

www.acsami.org

Multifunctional Hollow Mesoporous Silica Nanocages for Cancer Cell Detection and the Combined Chemotherapy and Photodynamic Therapy

Tingting Wang,[†] Lingyu Zhang,[†] Zhongmin Su,[*,†] Chungang Wang,[*,†] Yi Liao,[‡] and Qin Fu[§]

[†]Institute of Functional Material Chemistry, Faculty of Chemistry, Northeast Normal University, Changchun 130024, P. R. China

[‡]Department of Chemistry, Capital Normal University, Beijing 100048, P. R. China

[§]Jilin Province Institute of Cancer Research, Changchun 130012, P. R. China

Supporting Information

ABSTRACT: Highly uniform and multifunctional hollow mesoporous silica nanocages that combined excellent properties (good biocompatibility, fluorescence imaging, drug delivery, and dual-mode cancer therapy) in one single system were synthesized. Dye molecules labeled in the nanocages could be used as traceable detectors in fluorescence imaging. A chemotherapeutic drug, doxorubicin (DOX), has been loaded into the nanocages with a high storage capacity due to the large cubic cavities and could be released through the penetrating mesoporous channels in a sustained fashion. Hematoporphyrin molecules were also covalently doped in the nanocages and allowed for photodynamic therapy. More importantly, a cooperative, synergistic therapy combining chemotherapy and photodynamic therapy exhibited high therapeutic efficacy for cancer therapy in vitro.

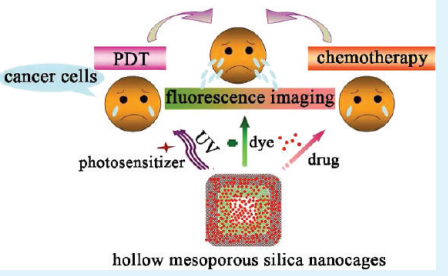

KEYWORDS: mesoporous silica nanocage, drug delivery, photodynamic therapy, sustained release, cancer therapy, fluorescence imaging

INTRODUCTION

Nanomaterials, because of their novel, intrinsic physical properties, have recently emerged as promising candidates for cancer diagnosis and therapy.[1−5] Among the reported cancer-related applications investigated to date, inorganic nanoparticles, with the desirable biocompatibility and through controllable synthesis coupled with rationally designed functionalization, have gain significant attention and offered a route toward multifunctional composite systems.[6−15] One interesting class of inorganic nanomaterials for potential medical applications is mesoporous silica nanoparticles (MSN). Because of the advantages of high surface area, tailorable pore size, controllable particle size and shape, and versatile surface modification, MSN provide a new platform for a range of applications, from improved cancer diagnosis, anticancer drug delivery, to targeted therapy.[4,16−20] However, hollow mesoporous silica nanoparticles (HMS) are more powerful, preferable, and suitable than these conventional MSN in the performance of cancer treatment, in particular to act as drug delivery carriers, because of the huge cavities inside the particles.[21−25] For example, in chemotherapy, one of the most well-established cancer treatments today, chemotherapeutic drugs are toxic and could cause side-effects by the nonspecific uptake by healthy cells. In contrast, HMS nanomaterials can be employed to load chemotherapeutic drugs with a high storage capacity and transport them to tumor site, effectively protecting the healthy cells from damages by these drugs. Besides, silica-based nanomaterials exhibit excellent performance in photodynamic therapy (PDT) by incorporating photosensitizers.[26−34] PDT is based on the concept that the photosensitizers become active and therefore generate singlet oxygen under irradiation with appropriate light wavelengths in the presence of molecular oxygen to induce tumor cell death. Many of the photosensitizers such as porphyrin-based molecules have a limited solubility in water and therefore easily aggregate in the physiological environment, which would limit their applications in PDT. To address these limitations, covalently incorporating the photosensitizers inside the silica matrices with rational coupling method can greatly enhance their water solubility and stability, avoid inactivation in the physiological environment, and particularly improve the accumulation of the photosensitizer drugs in the tumor site.[28,31]

On the other hand, the functionality of HMS nanomaterials can be extended from drug carriers in cancer therapy to simultaneous imaging diagnosis and therapy by encapsulating diverse functional moieties into the nanomaterials. Therefore, the nanoparticles are endowed with unique properties for traceable multi-imaging purposes, such as magnetic nanoparticles for magnetic resonance imaging, Au nanoparticles for two-photon

Received: March 23, 2011
Accepted: May 24, 2011
Published: May 24, 2011

ACS Publications © 2011 American Chemical Society

Scheme 1. Schematic Illustration of the Synthetic Process for FITC-HMS-HP Nanocages and Application in Cancer Cell Therapy As Drug Delivery Carriers[a]

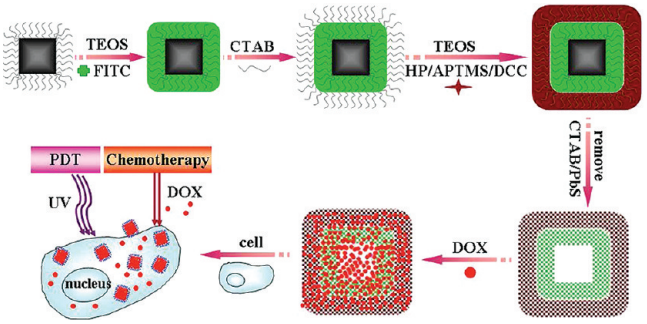

[a] TEOS: tetraethyl orthosilicate; APTMS: 3-aminopropyltrimethoxysilane; CTAB: cetyltrimethylammonium bromide; DCC: N,N′-dicyclohexyl carbodiimide; HP: hematoporphyrin; FITC: fluorescein isothiocyanate; DOX: doxorubicin hydrochloride.

imaging and Raman spectroscopy, quantum dots, and fluorescent molecules for fluorescence imaging.[2−4,18,23,28]

Breakthroughs have been made on the nanomaterial-based applications in cancer therapies (chemotherapy, PDT, photothermal therapy, etc.), especially on the use of the multifunctional silica-based materials. Recently, we have successfully synthesized monodisperse and uniform HMS nanocages via template-coating-etching process and investigated the therapeutic efficacy of anticancer drug-loaded HMS nanocages in vitro and in vivo for liver cancer therapy taking advantage of their high drug storage capacity.[35] However, to the best of our knowledge, investigations on a cooperative, synergistic therapy that combines two or multiple individual treatment into one system are seldom reported.[7,36−40] In this study, the focus is on the idea of a dual-mode therapeutic multifunctional nanocarrier system combining PDT and chemotherapy based on the HMS nanocages, as schematically shown in Scheme 1. The synthetic strategy for the formation of HMS nanocages possessing hollow cubic cores and mesoporous shells was based on a template-coating-etching process similar to our previous work.[35] Meanwhile, fluorescein isothiocyanate (FITC) and hematoporphyrin (HP) were covalently incorporated into silica walls as fluorescent detectors for fluorescence imaging. Finally, chemotherapeutic drugs doxorubicin (DOX), were successfully loaded into the nanocages with a significantly high drug storage capacity, benefiting from the ample loading space provided by the cubic cavities in the cores and the porous shells. In addition, HP molecules doped in silica shells acted as photosensitizers for PDT to initiate the generation of cytotoxic species, such as singlet oxygen ($^1O_2$) and other reactive oxygen species (ROS). In vitro cell assays demonstrated that the nanocages could be used as probes for fluorescence imaging and very promising biocompatible carriers for loading and delivery of chemotherapeutic drugs and photosensitizers to achieve an all-in-one system possessing cell imaging, drug loading and delivery, chemotherapy, and PDT functionalities.

EXPERIMENTAL SECTION

Materials and Measurements. 3-Aminopropyltrimethoxysilane (APTMS, 95%), N,N′-dicyclohexyl carbodiimide (DCC), tetraethyl orthosilicate (TEOS, ≥98%), cetyltrimethylammonium bromide (CTAB, ≥99%), fluorescein isothiocyanate (FITC), hematoporphyrin (HP), and 9,10-anthracenediyl-bis(methylene) dimalonic acid (ABDA) were purchased from Sigma (USA). Thioacetamide (TAA), acetic acid (HAc), lead acetate ($Pb(Ac)_2$) were purchased from Sinopharm Chemical Reagent Beijing Co. Ltd. Chemotherapeutic drug doxorubicin hydrochloride (DOX) were obtained from Shenzhen Main Luck Pharmaceuticals Inc.. All reagents were used as received. Deionized water (18.0 MΩ cm^{-1}) was used in all the experiments.

TEM was performed on a JEOL-2100F transmission electron microscope under 200 kV accelerating voltage. UV−vis absorption spectroscopy was obtained on U-3010 spectrophotometer (Hitachi, Japan). Fluorescence spectra were performed with Eclipse fluorescence spectrophotometer (Varian, USA). Confocal laser scanning microscopy (CLSM) was operated on Olympus Fluoview FV1000. FTIR spectra were obtained on a Magna560 FTIR spectrometer (Nicolet, USA). X-ray diffraction (XRD) patterns were obtained on a D8 Focus diffractometer (Bruker) with Cu−Kα radiation (λ = 0.15405 nm).

Synthesis of FITC-Modified Mesoporous Silica-Coated PbS Nanocubes (FITC-PbS@mSiO$_2$). The PbS nanoparticles with cubic morphology were synthesized according to a previous report.[41] In brief, 0.5 M TAA was added into an aqueous solution containing CTAB, HAc, and $Pb(Ac)_2$ at room temperature. In 20 mL of the resultant solution, the final concentration of CTAB, HAc, $Pb(Ac)_2$, and TAA were 5.7, 91.0, 22.7, and 80.0 mM, respectively. The mixture was then allowed to continuously stir at 80 °C for 24 h. The resultant black PbS nanocubes were purified by centrifugation and dispersed in 20 mL of deionized water for further use.

To incorporate FITC into silica matrices, we first covalently linked 4 mg of FITC to 44 μL of APTMS in 1 mL of ethanol overnight under dark conditions.[18] The FITC-PbS@mSiO$_2$ nanocubes were fabricated using a modified sol−gel method.[42] In a typical procedure, 11 mL of PbS nanocubes were centrifuged and redispersed in 22 mL of deionized water. Surfactant template CTAB (0.2 M, 8 mL) were added into PbS nanocube solution and stirred overnight. Then, 25 μL of the FITC-APTMS solution was injected into the solution after the pH value was adjusted to ∼11 with 0.1 M NaOH solution. After that, 100 μL of 20% TEOS in ethanol was injected seven times at a 30 min interval and subsequently stirred for 24 h at room temperature. The as-synthesized FITC-PbS@mSiO$_2$ nanocubes were washed with water twice to remove the unreacted species and redispersed in 48 mL of deionized water for further use.

Synthesis of HP-Doped FITC-Modified Hollow Mesoporous Silica Nanocages (FITC-HMS-HP). To dope hematoporphyrin (HP) into nanocages, HP molecules (10 mg) were first activated by DCC (3.54 mg) in DMF (1 mL) and then reacted with APTMS (5 μL) to obtain the HP-functionalized silanization precursor.[28] The as-synthesized FITC-PbS@mSiO$_2$ nanocubes (48 mL) were mixed with CTAB solution (0.2 M, 4 mL) for 4 h. Then, 300 μL of HP-functionalized silanization precursor and 700 μL of 20% TEOS in ethanol were added into the mixture under a pH value of ∼11 adjusted with 0.1 M NaOH at a 30 min interval. The reaction was allowed to further stir for 24 h. The product FITC-PbS@mSiO$_2$−HP nanocubes were collected by centrifugation and dispersed in 70 mL of ethanol. To remove CTAB molecules completely as well as PbS cores, we used HNO_3 for extraction and etching, resulting in FITC-HMS-HP nanocages. After washing them six times with ethanol and water to remove impurities, the FITC-HMS-HP nanocages were left to dry for further use. The supernatant of the solution was collected for the treatment to avoid contamination.

Cell Culture. MCF-7 cells, human breast cancer cell line, were maintained in iscove's modified dulbecco's medium (IMDM) supplemented with 10% fetal bovine serum in a humidified incubator in a 95% air/5% CO_2 atmosphere at 37 °C. For all experiments, cells were harvested by the use of trypsin and were resuspended in fresh complete medium before plating.

Cell Uptake. To observe cell uptake of FITC-HMS-HP nanocages, we first seeded 1.0×10^5 mL^{-1} MCF-7 cells onto a glass coverslip in a 24-well plate in IMDM medium containing 10% fetal bovine serum for 24 h at 37 °C in a humidified atmosphere with 5% CO_2 to permit cell attachment. Then the cells were incubated with FITC-HMS-HP nanocages (25 μg mL^{-1}, 1 mL) in serum-free medium for 24 h, followed by PBS wash several times to remove the remaining particles and dead cells. Subsequently, the cells were treated with Hoechst 33342 (10 μg mL^{-1}) for 20 min to stain the nuclei. The cells were washed with PBS to remove extra dye molecules and then sealed with a microscope glass slide. Observations were performed using a CLSM. The fluorescence signals of Hoechst 33342 (blue), FITC (green), and HP (red) were detected with 405, 488, and 543 nm excitation light, respectively.

Drug Loading and In vitro Release. UV−vis spectroscopy was used to determine the amount of doxorubicin (DOX) loaded into the nanocages. A stock solution of DOX (2 mg mL^{-1}) was serially diluted to concentrations of 10−120 μg mL^{-1} in deionized water. A standard curve was determined by taking the absorption intensity at 480 nm versus DOX concentration as parameters and presented a linear variation. In a typical procedure, the drug-loaded nanocages were prepared by mixing DOX aqueous solution (2 mg mL^{-1}, 50 μL) with FITC-HMS-HP nanocages (1.0 mg mL^{-1}, 1.0 mL) for 48 h and then centrifuged at 10 000 rpm for 20 min. To evaluate the DOX-loading efficiency (LE) and encapsulation content, we determined the content of the residual DOX in supernatant by UV−vis measurements at 480 nm and compared to the standard curve created previously. The DOX-loading efficiency was calculated by eq 1

$$\mathrm{LE}(\%) = [m_{(\text{total DOX})} - m_{(\text{DOX in supernatant})}]/m_{(\text{total DOX})} \times 100\% \quad (1)$$

In vitro DOX release from DOX-loaded FITC-HMS-HP nanocages was evaluated using a semipermeable dialysis bag diffusion technique right after the preparation of DOX-loaded nanocages. Two portions of the as-prepared DOX-loaded FITC-HMS-HP nanocages at equal amount were redispersed in 0.5 mL of PBS (pH 7.4) and 0.5 mL of acetate buffer (pH 5.1), respectively. Both of the release media were transferred into pretreated semipermeable dialysis bags and then immersed into 3 mL of deionized water at 37 °C with gentle shaking, respectively. At selected time intervals, the amount of released DOX moved out of semipermeable dialysis bag into water was measured by fluorescence spectrophotometer with emission at 591 nm and excitation at 479 nm.

Detection of Singlet Oxygen. Generation of singlet oxygen can be usually detected by the characteristic photoluminescence peak of singlet oxygen at 1270 nm or by chemical method using 1,3-diphenylisobenzofuran (DPBF) or 9,10-anthracenediyl-bis(methylene) dimalonic acid (ABDA) as a singlet oxygen sensor.[27,28] In our experiment, ABDA was chosen to monitor the release of singlet oxygen into solution by recording the decrease in absorption of ABDA at 376 nm via UV−vis spectroscopy. 50 μL of ABDA solution (2 mg mL^{-1}) was mixed well with FITC-HMS-HP (0.5 mg mL^{-1}, 600 μL) and DOX-loaded FITC-HMS-HP (0.5 mg mL^{-1}, 600 μL) and placed in a cuvette, respectively, whereas ABDA only in deionized water was used as control. The absorption intensity of ABDA at 376 nm was monitored under different UV illumination periods.

In vitro Chemotherapy and Photodynamic Therapy Studies. Cell cytotoxicity studies were determined by standard 3-(4,5-dimethylthialzol-2-yl)-2,5-diphenyltetrazolium bromide (MTT) assays and MCF-7 cells were used. To evaluate the biocompatibility and cytotoxicity of FITC-HMS-HP nanocages, we seeded cells in a 96-well plate at a density of 2.5×10^4 mL^{-1} (100 μL) per well and incubated at 37 °C in a humidified atmosphere with 5% CO_2 in IMDM medium containing 10% fetal bovine serum for 24 h to attach. The cells were then incubated with various concentrations of FITC-HMS-HP nanocages for 24 h. One row of 96-well plate was used as control with culture medium only. After this incubation, 20 μL 5 mg mL^{-1} MTT solution was added to each well and the mixture was incubated for another 4 h. The amount of dark-blue formazan crystals generated by the live cells was proportional to the number of live cells. Thereafter, the medium was replaced with DMSO (150 μL) and the absorbance was monitored with a microplate reader at a wavelength of 490 nm. Cell viability was determined by eq 2

$$\text{Cell Viability}(\%) = \mathrm{Abs}_{(\text{test cells})}/\mathrm{Abs}_{(\text{reference cells})} \times 100\% \quad (2)$$

For control experiments, cells were exposed to UV illumination for different periods (20, 40, and 60 min) without treatment with FITC-HMS-HP nanocages and the cell viability was measured with MTT assay. The phototoxicity effect of FITC-HMS-HP nanocages on MCF-7 cells was tested by treating with FITC-HMS-HP nanocages at different concentrations and illuminating under UV light for different periods (20, 40, and 60 min). For chemotherapy and photodynamic therapy studies, cells were treated with serial concentrations (6.25, 12.5, 25, 50, and 100 μg nanocages mL^{-1}) of free DOX, DOX-loaded FITC-HMS-HP nanocages, empty FITC-HMS-HP and UV illuminating for 60 min, DOX-loaded FITC-HMS-HP and UV illuminating for 60 min, respectively, and the cell viability was measured with MTT assay described previously. The concentrations of free DOX were set at the same level as the DOX concentrations in the DOX-loaded groups (0.58, 1.15, 2.3, 4.6, 9.2 μg DOX mL^{-1}). 365 nm UV light was used in the above experiments and the intensity of the 365 nm UV light was 380 μW cm^{-2} measured by a ultraviolet ray intensity meter Trina TN-2340.

RESULTS AND DISCUSSION

Synthesis and Characterization of FITC-HMS-HP Nanocages. Monodisperse and uniform HMS nanocages with cubic hollow cores were synthesized via a template-coating-etching process where cetyltrimethylammonium bromide (CTAB) were used as pore-generating templates and PbS nanocubes were used as hollow cubic core-generating templates. The initial PbS nanocubes capped with surfactant CTAB molecules were synthesized via aqueous solution routes using $Pb(Ac)_2$ and TAA as precursors. In this procedure, CTAB served not only as a capping agent for influencing the morphology of PbS nanocubes, but also as the structure-directing agent for the formation of mesoporous silica coatings. Before adding silica precursor tetraethyl orthosilicate (TEOS), an additional CTAB solution was mixed with the as-prepared PbS nanocubes to provide sufficient CTAB molecules localized on the nanocube surfaces which may promote the mesoporous silica shell growth. The PbS nanocubes were subsequently coated with mesoporous silica shells (PbS@mSiO_2) via base-catalyzes hydrolysis of TEOS and condensation of silica onto the surface of the CTAB molecules. Meanwhile, fluorescent dye molecules fluorescein isothiocyanate (FITC) treated with 3-aminopropyltrimethoxysilane (APTMS) in advance were also functionalized covalently into the silica walls by carrying out a silica sol−gel reaction during the PbS@mSiO_2 synthesis step. After washing step, FITC-labeled PbS@mSiO_2 nanocubes presented a negatively charged surface and then redispersed in CTAB solution to load positively charged CTAB molecules. CTAB were once again used as pore-generating templates for the formation of the second mesoporous silica layers which the photosensitizer molecules hematoporphyrin (HP) were doped in. To effectively dope HP into HMS nanocages, we first incorporated HP molecules with APTMS to obtain HP-functionalized silanization precursor and subsequently injected with TEOS to form HP-doped mesoporous silica shells via a second sol−gel co-condensation process.

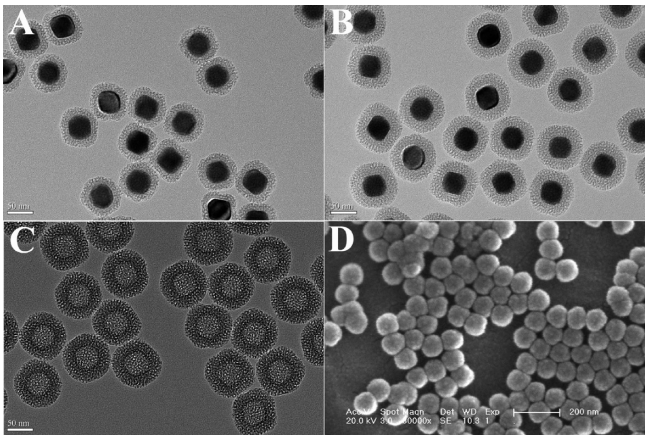

Figure 1. TEM images of (A) FITC-labeled PbS@mSiO$_2$ nanocubes, (B) HP-doped FITC-labeled PbS@mSiO$_2$ nanocubes, (C) FITC-HMS-HP nanocages, and (D) FE-SEM image of FITC-HMS-HP nanocages. Scale bars for A−C are 50 nm.

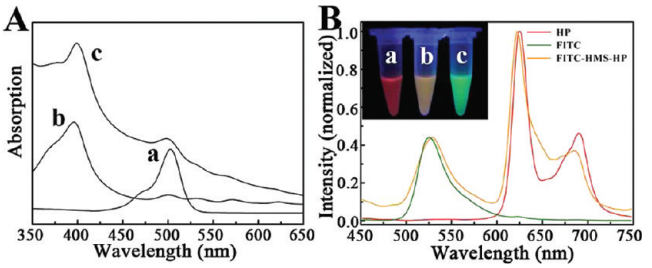

Figure 2. (A) UV−vis absorption spectra of (a) free FITC, (b) free HP, and (c) FITC-HMS-HP nanocages. (B) Photoluminescence spectra of (green) free FITC, (red) free HP, and (yellow) FITC-HMS-HP nanocages (λ_{ex} = 390 nm). Inset: digital photographs of (a) free HP, (b) FITC-HMS-HP nanocages, and (c) free FITC under UV light.

In order to evolve FITC-HMS-HP nanocages with hollow cubic cores and penetrating pore channels, ethanol and HNO_3 were utilized to remove CTAB pore-generating templates and PbS core-generating templates completely. After thoroughly washing with ethanol and water, FITC-HMS-HP nanocages were finally created with no aggregation and precipitation. The supernatant of solution was collected for the treatment to avoid contamination.

Figure 1A shows the TEM image of FITC-labeled PbS@mSiO$_2$ nanocubes possessing a cubic PbS core with an average diameter of 42 ± 2 nm and a uniform silica shell (ca. 14 ± 2 nm) composed of mesopores. After doping HP molecules, the thickness of the mesoporous shell was increased to ca. 24 ± 2 nm (Figure 1B). Images C and D in Figure 1 show the TEM and FE-SEM images of FITC-HMS-HP nanocages, displaying the central hollow cubic cores (ca. 42 ± 2 nm) and wormhole-like mesoporous silica shells (ca. 24 ± 2 nm) generated by the removal of core and pore templates. Figure S1 in the Supporting Information shows that the nanocages had a narrow size distribution in water measured by dynamic light scattering (DLS). These nanocages are quite uniform, stable and monodisperse in water and even in culture medium IMDM without detectable aggregation (see Figure S2 in the Supporting Information). The wide- and small-angle XRD patterns reveal that the amorphous mesoporous silica shells are composed of disordered pores, similar to previous works (see Figure S3 in the Supporting Information).[42,43] Such a hollow mesoporous structure would greatly enhance the drug loading capacity, because drug molecules can not only storage in the mesoporous channels but also in the large cubic cavities in the center. Furthermore, HP molecules, which have been utilized as photosensitizer drugs in photodynamic therapy (PDT), were covalently incorporated in silica matrices. Therefore, FITC-HMS-HP nanocages were highly desirable for anticancer drug delivery in both cancer cell chemotherapy and PDT. Although Pb ion is toxic, there are still some special advantages for PbS as templates. (i) The synthetic process of PbS nanocubes is simple and reproducible. (ii) The mesoporous silica shells can be easily formed with a unique cubic shape due to the CTAB-capped surface and cubic morphology of PbS nanocubes. The PbS nanocubes coated with mesoporous silica shells and the final products HMS nanocages are quite monodisperse and uniform, as shown in TEM images. (iii) The average size of PbS nanocubes is less than 50 nm. Mou and his coworkers have reported that cancer cell uptake is particle-size-dependent and the maximum uptake occurs at a nanoparticle size less than 100 nm.[44] Thus, it is further demonstrated that the PbS nanocubes can provide acceptable size as template for the formation of HMS nanocage. In addition, the energy-dispersive X-ray spectrum (EDS) of the as-prepared FITC-HMS-HP nanocages shows that there was no residue of PbS in the HMS nanocages (see Figure S4 in the Supporting Information), indicating that the potential side effect caused by PbS can be avoided effectively.

To endow HMS nanocages with multifunctionalities in the biomedical applications of cancer imaging and therapy, the fluorescence imaging agents FITC with the photosensitizer molecules HP were combined within the same HMS nanocages. In the experimental procedure, FITC and HP molecules were covalently doped in two different mesoporous silica layers by using sol−gel reaction in two-step process. It could maximally incorporate FITC and HP molecules into the nanocages by avoiding the steric hindrance. On the other hand, FITC molecules were partially separated from HP by the two silica coatings, which could reduce the unpredictable perturbations to the photosensitizer molecules. The loading concentrations of FITC and HP inside the nanocages are about 0.010 μmol and 0.056 μmol per mg nanocages, respectively, estimated by UV−vis absorption spectroscopy. Panels A and B in Figure 2 show the UV−vis absorption spectra and fluorescence spectra of free FITC, free HP, and FITC-HMS-HP nanocages, respectively. It can be seen that both the absorption bands and fluorescence peaks of FITC-HMS-HP nanocages very coincide with those of free FITC and HP and are almost unchanged. Under UV light excitation, free HP and FITC molecules exhibited brightly red and green colors, respectively, whereas FITC-HMS-HP nanocages displayed yellow color due to the mixing of red from HP molecules and green from FITC molecules (the inset of Figure 2B). These results further demonstrate that FITC and HP have been effectively incorporated in the HMS nanocages and can be used as detectors in fluorescence imaging.

Biocompatibility and Cell Uptake of FITC-HMS-HP Nanocages. The study on biocompatibility and cytotoxicity of drug delivery vehicles is very important for drug delivery systems. In vitro cytotoxicity of FITC-HMS-HP nanocages against MCF-7 cells were conducted by MTT assays. Figure 3 shows that FITC-HMS-HP nanocages at different concentrations have no cytotoxic effect on cell viability, even at a high concentration up to 200 μg mL^{-1}. The results prove that the nanocages have good

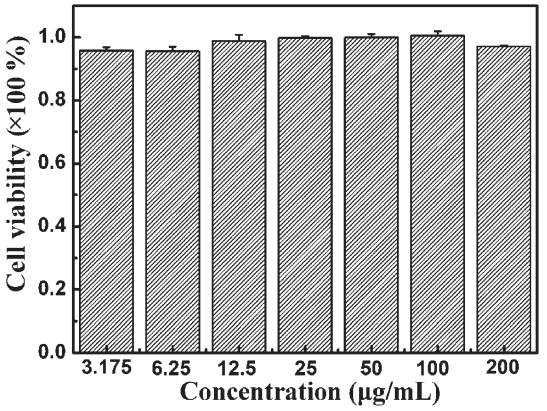

Figure 3. In vitro cytotoxicity of FITC-HMS-HP nanocages against MCF-7 cells at different concentrations after 24 h incubation.

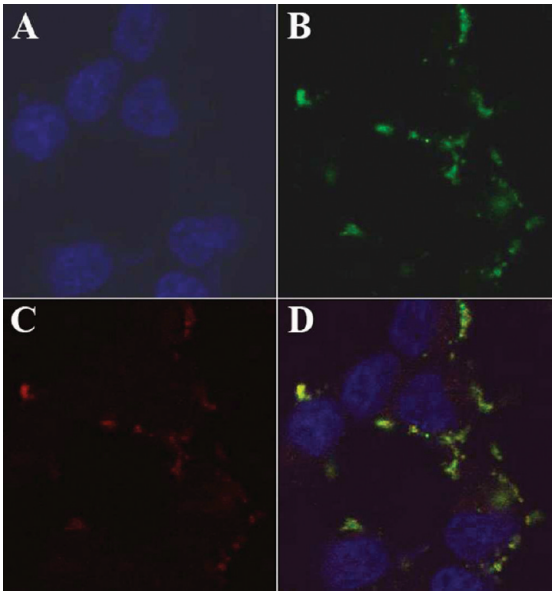

Figure 4. Confocal laser scanning microscopic images of MCF-7 cells incubates with FITC-HMS-HP nanocages for 24 h. (A) Nuclei stained with blue Hoechst 33342; (B, C) fluorescence signals of FITC and HP of FITC-HMS-HP nanocages, shown in green and red color, respectively; (D) merged image of blue (Hoechst 33342), green (FITC), and red (HP).

biocompatibility and would be promising carriers in practical cancer therapy applications.

Good cell uptake of carriers is also very vital for cancer diagnosis. On one hand, it can guarantee the delivery efficiency as a drug-delivery system and achieve the desired therapeutic effect. On the other hand, it can facilitate the application of traceable imaging of nanoparticles in cancer cell diagnosis accomplished by directly incorporating fluorescence imaging agents. Cell uptake of FITC-HMS-HP nanocages was verified by confocal laser scanning microscopy (CLSM) following the incubation of MCF-7 cells with the nanocages in cell culture medium for 24 h. The cell nuclei were stained with Hoechst 33342 (Figure 4A). As shown in Figure 4B, the spotlike green fluorescence emitted by FITC from the nanocages was observed inside the cytoplasmic regions of the cells, implying that a substantial fraction of nanocages were internalized via endocytosis. HP molecules, a particular class of anticancer drugs, are usually used as photosensitizers and therefore cytotoxic only when excited at precise frequencies in the presence of molecular oxygen.[6] Interestingly, as HP are fluorescent molecules, they can also offer a means for cell imaging. The image in Figure 4C exhibiting the red fluorescence was attributed to the presence of HP molecules in nanocages. In the merged image of Figure 4D, it can be seen that the location of red-emitting points of HP coincided with that of FITC, suggesting that the successful cell uptake of nanocages can be verified in two modes by CLSM.

Capability of FITC-HMS-HP Nanocages as Chemotherapeutic Drug Delivery System. Nanoparticles are more and more employed as therapeutic drug carriers in recent researches, attributing to the high loading dose and sustained therapy efficiency, and can effectively protect the healthy tissues/organs and prevent the severe side-effect from the toxic drugs by nonspecific uptake.[23] The loading capacity and release property of FITC-HMS-HP nanocages as drug delivery systems were investigated by spectroscopy technology, and a water-soluble chemotherapeutic drug, doxorubicin hydrochloride (DOX) has been chosen as a model drug. Figure 5A shows the UV−vis absorption spectra of DOX solution before and after the interaction with FITC-HMS-HP nanocages, respectively. DOX molecules could be successfully loaded into the nanocages, evidenced by the significant decrease of the absorption intensity of the initial DOX solution in a corresponding volume and the reddish color of the nanocages due to the absorbed DOX. The drug loading efficiency could reach 92% and the drug loading content was 92 μg DOX mg^{-1} supports, when 2 mg mL^{-1} 50 μL initial

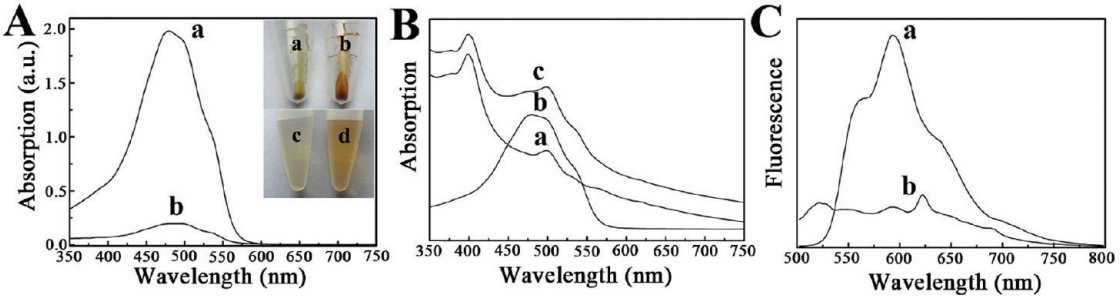

Figure 5. (A) UV−vis absorption spectra of (a) DOX solutions before and (b) the residual DOX content in the supernatant after interaction with FITC-HMS-HP nanocages. Inset: digital photographs of (a) DOX-unloaded FITC-HMS-HP nanocages, (b) DOX-loaded FITC-HMS-HP nanocages, (c, d) corresponding dispersion images of a and b, respectively. (B) UV−vis absorption spectra of (a) free DOX, (b) FITC-HMS-HP nanocages, and (c) DOX-loaded FITC-HMS-HP nanocages. (C) Fluorescence spectra of (a) free DOX and (b) DOX-loaded FITC-HMS-HP nanocages.

DOX solution interacted with 1 mg nanocages. In addition, UV−vis spectrum of DOX-loaded nanocages reveals DOX peaks superimposing with the curve of nanocages (Figure 5B). Moreover, a high degree quenching of DOX fluorescence was observed after loading in nanocages, compared with the strong emission of free DOX when excited at 479 nm (Figure 5C). The high concentration of DOX loaded in nanocages may induce concentration quenching including radiationless transfer of energy between DOX molecules, resulting in the DOX fluorescence quenching. On the basis of these results, we confirm that drugs can be loaded into the nanocages. Being a drug delivery system, FITC-HMS-HP nanocages showed a high loading capacity attributing to the larger space for storing drug molecules, provided by the huge cavities in the cores and the mesoporous shells. Drug molecules can diffuse into the nanocages through pore channels to reach a maximum storage capacity as long as they can gain access to the interior cavities.[22]

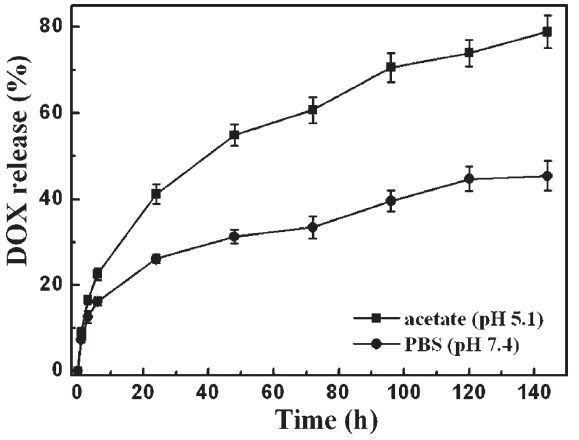

Figure 6. DOX-release profiles for DOX-loaded FITC-HMS-HP nanocages measured at pH 5.1 in acetate buffer and at pH 7.4 in PBS buffer at 37 °C, respectively.

It is commonly accepted that mesoporous materials possess sustained drug release property.[23] The release profiles of DOX from DOX-loaded FITC-HMS-HP nanocages over a 144 h period in two different pH conditions at 37 °C are shown in Figure 6. Regardless the pH value, the DOX-loaded nanocages obviously have a sustained release property. A relative fast release happened within 8 h and a sustained release followed until the end of the assay. Therefore, it would be useful for the cancer treatment by chemotherapy requiring a high initial dose and continuous therapy efficiency without frequent interval medication administrations. It is interesting to note that the DOX release rate was faster at mildly acidic pH than at neutral pH. Approximately 41% of DOX was released with 24 h at pH 5.1 in acetate buffer, whereas no less than 30% was released at pH 7.4 in PBS buffer. This trend was ascribed to the increased hydrophilicity and higher solubility of DOX at lower pH caused by increased protonated $-NH_2$ groups on DOX. This kind of kinetics implies that drug molecules could be released preferentially in the mild acidic environments of tumor areas, where the pH is less than the physiologically neutral pH of normal tissue or biological fluids.[13,45]

Capability of Singlet Oxygen Generation of FITC-HMS-HP Nanocages. High singlet oxygen generation efficiency is an important requirement for application of photosensitizers in PDT. To verify the generation of singlet oxygen produced by FITC-HMS-HP nanocages, a chemical method was used by the photo-oxidation of ABDA to form an endoperoxide, which caused a decrease in ABDA absorption intensity at 376 nm. As shown in Figure 7B, the results indicate that the absorption intensity of ABDA gradually decreased over the course of UV illumination in the presence of FITC-HMS-HP nanocages, suggesting an increase amount of singlet oxygen produced by the HP-doped nanocages. In contrast, the change of the absorption intensity of ABDA was negligibly small in the absence of FITC-HMS-HP nanocages under the same experiment condition in the control experiment, confirming that the decrease in absorption of ABDA was a result of a combined effect of FITC-

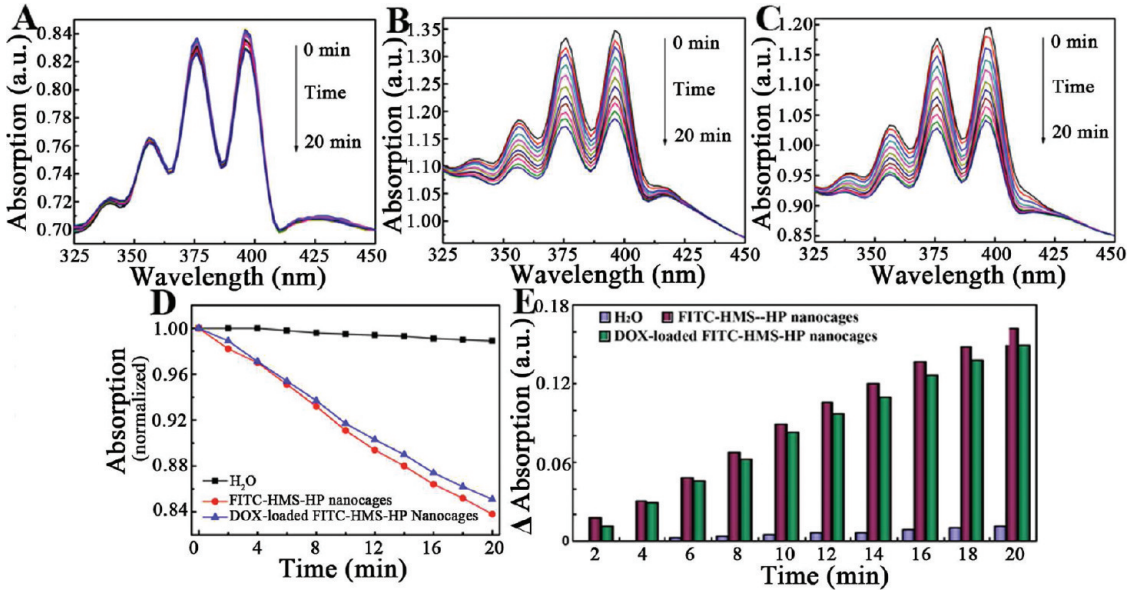

Figure 7. Photobleaching of ABDA by singlet oxygen generated by (A) water alone as control, (B) FITC-HMS-HP solution, and (C) DOX-loaded FITC-HMS-HP solution. (D) Decay curves of ABDA absorption at 376 nm as a function of illumination time, corresponding to A−C. (E) Time-dependent decrease in ABDA absorption (ΔA) as a function of illumination time, corresponding to A−C.

HMS-HP nanocages and the UV illumination but not the illumination itself (Figure 7A). The capability of DOX-loaded FITC-HMS-HP nanocages to generate singlet oxygen was also monitored under the same condition. There was a continuous decrease in the absorption of ABDA with the increase of illumination time by UV light, shown in Figure 7C. Although DOX molecules have been loaded in the nanocages, the capability of singlet oxygen generation of HP doped in the nanocages was not influenced by DOX. However, the photo-oxidation efficiency of DOX-loaded FITC-HMS-HP nanocages was slightly lower than that of DOX-unloaded group, which is due to the loading of DOX may to some extent block the release of singlet oxygen to the surrounding environment. Panels D and E in Figure 7 are also plotted for intuitive comparison, respectively, showing that the absorption of ABDA is time-dependent under UV illumination in the presence of FITC-HMS-HP nanocages. Thus, it is suggested that the nanocages can act as multidrug delivery carriers not only for chemotherapeutic drugs but also for the photosensitizer drugs.

In vitro Cytotoxicity of DOX-loaded FITC-HMS-HP Nanocages. The photodynamic activity of FITC-HMS-HP nanocages toward MCF-7 cells was first measured using the MTT assays. Figure S5 shows that the FITC-HMS-HP nanocages at higher dosage and under longer UV exposure time can lead to more cytotoxicity on cells, exhibiting a dosage- and time-dependent tendency on cell viability (Supporting Information). The illumination of MCF-7 cells alone without the treatment of FITC-HMS-HP nanocages under UV light was used as control and did not induce any significant toxicity (see Figure S6 in the Supporting Information). In addition, it is known that FITC-HMS-HP nanocages are satisfactory biocompatible and nontoxic incubated with cells without UV illumination as discussed in Figure 3. These results suggest that the cytotoxic effect on cancer cells is caused by FITC-HMS-HP nanocages and UV illumination together, but neither FITC-HMS-HP alone nor UV illumination alone. Second, to verify whether the released DOX from the FITC-HMS-HP nanocages was still pharmacologically active, the cytotoxic effect against MCF-7 cells was also investigated. As shown in Figure 8, DOX-loaded nanocages induced the MCF-7 cell death comparatively to free DOX under the same drug dosage and the cytotoxic efficacy was enhanced with an increase in their concentration. The cytotoxic effect of DOX-loaded nanocages probably is due to the inside release of DOX within the cells after the cell uptake. Third, a cooperative therapy combining chemotherapy and PDT was studied by treating cancer cells MCF-7 with both DOX-loaded FITC-HMS-HP nanocages and UV illumination. As shown in Figure 8, the combined treatment generated a significant cell death at different concentrations, compared with free DOX, DOX-loaded FITC-HMS-HP nanocages, and FITC-HMS-HP nanocages with UV illumination. Therefore, it suggests that cooperative, synergistic therapies using dual or multiple therapy types can produce remarkable therapeutic efficacy and help various types of therapies effectively play coordinate roles in cancer therapy. Herein, we used a relatively ineffecting light source (UV light) to prove the PDT concept and the synergistic therapy application, which is usually used for superficial skin diseases. While, the most commonly used light sources are lasers in PDT. To reach a deeper penetration depth and destroy the deep tumor tissue in the practical applications of PDT, a photosensitizer drug with red-light excitation and a laser with an appropriate wavelength are much better.

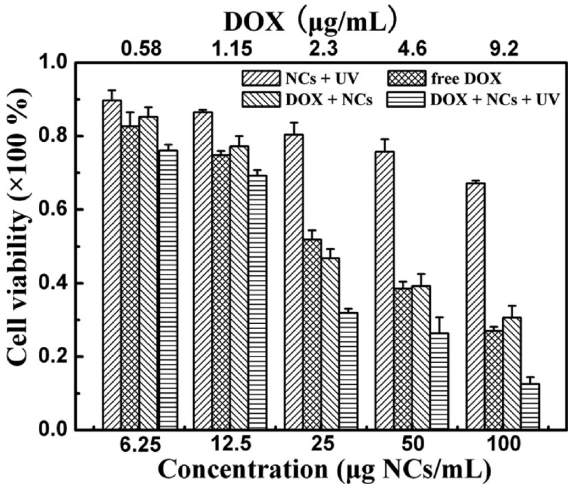

Figure 8. Viability of MCF-7 cells treated with both FITC-HMS-HP nanocages and UV, free DOX, DOX-loaded FITC-HMS-HP nanocages, and both DOX-loaded FITC-HMS-HP nanocages and UV at different concentrations, respectively. The exposure time with UV light is 60 min in the corresponding UV-treated groups. FITC-HMS-HP nanocages are abbreviated to NCs in this graph.

CONCLUSIONS

In conclusion, we have synthesized highly uniform, monodisperse, and multifunctional hollow mesoporous silica nanocages that comprise fluorescence imaging agent for optical tracking, photosensitizers for PDT, and huge cavities and penetrating pore channels for drug storage and sustained release. The multifunctional nanocages exhibited good biocompatibility for, and cell uptake by, cancer cells, which can guarantee the therapeutic efficacy as well as facilitate the application of traceable imaging. In vitro cancer therapy of the drug-loaded nanocages was evaluated. The results demonstrated that a cooperative therapeutic system combining chemotherapy and PDT can produce remarkable therapeutic efficacy relative to the individual means. The above consequences are the main contributions of our present work and provide a base for further study. More in-depth studies are needed before FITC-HMS-HP nanocages being used to clinical applications. For example, because of the versatile surface modification and nontoxic nature of silica matrices, FITC-HMS-HP nanocages are highly desirable for further targeting modality functionalized with active recognition moieties (such as tumor cell-specific targeting ligands or antibodies), which can more effectively improve drug-loaded nanocages accumulation in the tumor site and protect the normal organs and healthy cells from the toxic drugs. In addition, treatment conditions (the amounts of photosensitizer drug and chemotherapeutic drug, irradiation time) are very significant for practical applications and should be optimized to obtain a best synergistic effect, and thus, further in vivo studies are under way.

ASSOCIATED CONTENT

Supporting Information. Figure S1, size distribution of FITC-HMS-HP nanocages in water by dynamic light scattering; Figure S2, TEM image of FITC-HMS-HP nanocages in culture medium IMDM; Figure S3, XRD patterns of FITC-HMS-HP nanocages; Figure S4, EDS spectrum of FITC-HMS-HP nanocages; Figure S5, viability of MCF-7 cells treated with different

concentrations of FITC-HMS-HP nanocages and under different UV illumination time; Figure S6, viability of MCF-7 cells without the treatment of FITC-HMS-HP nanocages only under UV illumination for different times used as control. This material is available free of charge via the Internet at http://pubs.acs.org.

AUTHOR INFORMATION

Corresponding Author
*E-mail: zmsu@nenu.edu.cn (Z.S.); wangcg925@nenu.edu.cn (C.W.).

ACKNOWLEDGMENT

The authors gratefully acknowledge the financial support from the National High Technology Research and Development Program of China (Grant 2007AA03Z354), the Program for Changjiang Scholars and Innovative Research Team in University of Ministry of Education of China (Grant IRT0714), the National Natural Science Foundation of China (Project 20703009), the Fundamental Research Funds for the Central Universitiey (10JCXK004 and 10JCXK006) and the Science and Technology Development Planning of Jilin Province (20100929 and 20100320).

REFERENCES

(1) Cho, K.; Wang, X.; Nie, S. M.; Chen, Z.; Shin, D. M. *Clin. Cancer Res.* **2008**, *14*, 1310–1316.
(2) Park, K.; Lee, S.; Kang, E.; Kim, K.; Choi, K.; Kwon, I. C. *Adv. Funct. Mater.* **2009**, *19*, 1553–1566.
(3) Kim., J.; Piao, Y. Z.; Hyeon, T. *Chem. Soc. Rev.* **2009**, *38*, 372–390.
(4) Taylor-Pashow, K. M. L.; Rocca, J. D.; Huxford, R. C.; Lin, W. B. *Chem. Commun.* **2010**, *46*, 5832–5849.
(5) Chatterjee, D. K.; Fong, L. S.; Zhang, Y. *Adv. Drug Delivery Rev.* **2008**, *60*, 1627–1637.
(6) Minelli, C.; Lowe, S. B.; Stevens, M. M. *Small* **2010**, *6*, 2336–2357.
(7) Guo, R.; Zhang, L. Y.; Qian, H. Q.; Li, R. T.; Jiang, X. Q.; Liu, B. R. *Langmuir* **2010**, *26*, 5428–5434.
(8) Guo, Y.; Shi., D. L.; Cho, H.; Dong, Z. Y.; Kulkarni, A.; Pauletti, G. M.; Wang, W.; Lian, J.; Liu, W.; Ren, L.; Zhang, Q. Q.; Liu, G. K.; Huth, C.; Wang, L. M.; Ewing, R. C. *Adv. Funct. Mater.* **2008**, *18*, 2489–2497.
(9) You, J.; Zhang, G. D.; Li, C. *ACS Nano* **2010**, *4*, 1033–1041.
(10) Tang, S. H.; Huang, X. Q.; Chen, X. L.; Zheng, N. F. *Adv. Funct. Mater.* **2010**, *20*, 2442–2447.
(11) Lin, M. M.; Kim, H. H.; Kim, H.; Dobson, J.; Kim, D. K. *Nanomedicine* **2010**, *5*, 109–133.
(12) Huang, Y. F.; Sefah, K.; Bamrungsap, S.; Chang, H. T.; Tan, W. H. *Langmuir* **2008**, *24*, 11860–11865.
(13) Yu, M. Y.; Jeong, Y. Y.; Park, J.; Park, J.; Park, S.; Kim, J. W.; Min, J. J.; Kim, K.; Jon, S. *Angew. Chem., Int. Ed.* **2008**, *47*, 5362–5365.
(14) Liao, Z. Y.; Wang, H. J.; Lv, R. C.; Zhao, P. Q.; Sun, X. Z.; Wang, S.; Su, W. Y.; Niu, R. F.; Chang, J. *Langmuir* **2011**, *27*, 3100–3105.
(15) Wang, H.; Xu, J.; Wang, J. H.; Chen, T.; Wang, Y.; Tan, Y. W.; Su, H. B.; Chan, L. L.; Chen, H. Y. *Angew. Chem., Int. Ed.* **2010**, *49*, 8426–8430.
(16) Kim, J.; Kim, H. S.; Lee, N.; Kim, T.; Kim, H.; Yu, T.; Song, I. C.; Moon, W. K.; Hyeon, T. *Angew. Chem., Int. Ed.* **2008**, *47*, 8438–8441.
(17) Slowing, I. I.; Trewyn, B. G.; Giri, S.; Lin, V. S. Y. *Adv. Funct. Mater.* **2007**, *17*, 1225–1236.
(18) Lee, J. E.; Lee, N.; Kim, H.; Kim, J.; Choi, S. H.; Kim, J. H.; Kim, T.; Song, I. C.; Park, S. P.; Moon, W. K.; Hyeon, T. *J. Am. Chem. Soc.* **2010**, *132*, 552–557.
(19) Lu, F.; Wu, S. H.; Hung, Y.; Mou, C. Y. *Small* **2009**, *5*, 1408–1413.
(20) Lu, J.; Liong, M.; Li, Z. X.; Zink, J. I.; Tamanoi, F. *Small* **2010**, *6*, 1794–1805.
(21) Zhu, Y. F.; Ikoma, T.; Hanagata, N.; Kaskel, S. *Small* **2010**, *6*, 471–478.
(22) Zhao, W. R.; Chen, H. R.; Li, Y. S.; Li, L.; Lang, M. D.; Shi, J. L. *Adv. Funct. Mater.* **2008**, *18*, 2780–2788.
(23) Chen, Y.; Chen, H. R.; Zeng, D. P.; Tian, Y. B.; Chen, F.; Feng, J. W.; Shi, J. L. *ACS Nano* **2010**, *4*, 6001–6013.
(24) Zhu, Y. F.; Fang, Y.; Kaskel, S. *J. Phys. Chem. C* **2010**, *114*, 16382–16388.
(25) Chen, Y.; Chen, H. R.; Ma, M.; Chen, F.; Guo, L. M.; Zhang, L. X.; Shi, J. L. *J. Mater. Chem.* **2011**, *21*, 5290–5298.
(26) Cheng, S. H.; Lee, C. H.; Yang, C. S.; Tseng, F. G.; Mou, C. Y.; Lo, L. W. *J. Mater. Chem.* **2009**, *19*, 1252–1257.
(27) Tu, H. L.; Lin, Y. S.; Lin, H. Y.; Hung, Y.; Lo, L. W.; Chen, Y. F.; Mou, C. Y. *Adv. Mater.* **2009**, *21*, 172–177.
(28) Zhao, T. T.; Wu, H.; Yao, S. Q.; Xu, Q. H.; Xu, G. Q. *Langmuir* **2010**, *26*, 14937–14942.
(29) Zhang, R. R.; Wu, C. L.; Tong, L. L.; Tang, B.; Xu, Q. H. *Langmuir* **2009**, *25*, 10153–10158.
(30) Cheng, S. H.; Lee, C. H.; Chen, M. C.; Souris, J. S.; Tseng, F. G.; Yang, C. S.; Mou, C. Y.; Chen, C. T.; Lo, L. W. *J. Mater. Chem.* **2010**, *20*, 6149–6157.
(31) Couleaud, P.; Morosini, V.; Frochot, C.; Richeter, S.; Raehm, L.; Durand, J. O. *Nanoscale* **2010**, *2*, 1083–1095.
(32) Brevet, D.; Gary-Bobo, M.; Raehm, L.; Richeter, S.; Hocine, O.; Amro, K.; Loock, B.; Couleaud, P.; Frochot, C.; Morère, A.; Maillard, P.; Garcia, M.; Durand, J. O. *Chem. Commun.* **2009**, 1475–1477.
(33) Yang, Y.; Song, W. X.; Wang, A. H.; Zhu, P. L.; Fei, J. B.; Li, J. B. *Phys. Chem. Chem. Phys.* **2010**, *12*, 4418–4422.
(34) Hocine, O.; Gary-Bobo, M.; Brevet, D.; Maynadier, M.; Fontanel, S.; Raehm, L.; Richeter, S.; Loock, B.; Couleaud, P.; Frochot, C.; Charnay, C.; Derrien, G.; Smaïhi, M.; Sahmoune, A.; Morère, A.; Maillard, P.; Garcia, M.; Durand, J. O. *Int. J. Pharm.* **2010**, *402*, 221–230.
(35) Wang, T. T.; Chai, F.; Fu, Q.; Zhang, L. Y.; Liu, H. Y.; Li, L.; Liao, Y.; Su, Z. M.; Wang, C. G.; Duan, B. Y.; Ren, D. X. *J. Mater. Chem.* **2011**, *21*, 5299–5306.
(36) Park, H.; Yang, J.; Lee, J.; Haam, S.; Choi, I. H.; Yoo, K. H. *ACS Nano* **2009**, *3*, 2919–2926.
(37) Park, J. H.; Maltzahn, G. V.; Xu, M. J.; Fogal, V.; Kotamraju, V. R.; Ruoslahti, E.; Bhatia, S. N.; Sailor, M. *J. Proc. Natl. Acad. Sci. U.S.A.* **2010**, *107*, 981–986.
(38) Jang, B.; Park, J. Y.; Tung, C. H.; Kim, I. H.; Choi, Y. *ACS Nano* **2011**, *5*, 1086–1094.
(39) Khdair, A.; Chen, D.; Patil, Y.; Ma, L.; Dou, P.; Shekhar, M. P. V.; Panyam *J. Controlled Release* **2010**, *141*, 137–144.
(40) Khdair, A.; Handa, H.; Mao, G. Z.; Panyam, J. *Eur. J. Pharm. Biopharm.* **2009**, *71*, 214–222.
(41) Zhao, Z. H.; Zhang, K.; Zhang, J. H.; Yang, K.; He, C. Z.; Dong, F. X.; Yang, B. *Colloids Surf., A: Physicochem. Eng. Aspects* **2010**, *355*, 114–120.
(42) Gorelikov, I.; Matsuura, N. *Nano Lett.* **2008**, *8*, 369–373.
(43) Kim, J.; Lee, J. E.; Lee, J.; Yu, J. H.; Kim, B. C.; An, K.; Hwang, Y.; Shin, C. H.; Park, J. G.; Kim, J.; Hyeon, T. *J. Am. Chem. Soc.* **2006**, *128*, 688–689.
(44) Lu, F.; Wu, S. H.; Hung, Y.; Mou, C. Y. *Small* **2009**, *5*, 1408–1413.
(45) Huang, C. C.; Huang, W.; Yeh, C. S. *Biomaterials* **2011**, *32*, 556–564.